Available online at www.sciencedirect.com
ScienceDirect
Nuclear Physics B Proceedings Supplement 00 (2014) 1–6
Nuclear Physics B Proceedings Supplement

Pavel Krokovny

Budker Institute of Nuclear Physics and Novosibirsk State University

Abstract

We report the recent results on quarkonium (-like) states by the Belle experiment. A new charged charmonium-like state $Z_c(4200)^+$ decaying to $J/\psi\pi^+$ is observed with a significance of 6.2σ. The mass and width of the $Z_c(4200)^+$ are 4196^{+31+17}_{-29-13} MeV/c^2 and $370^{+70+70}_{-70-132}$ MeV, respectively; the preferred assignment of the quantum numbers is $J^P = 1^+$. We also report the first observation of the $e^+e^- \to \omega[\pi^+\pi^-\pi^0]\chi_{bJ}$ ($J = 1,\ 2$) processes at a center-of-mass energy of 10.867 GeV. In the $\pi^+\pi^-\pi^0$ invariant mass spectrum, significant non-ω signals are also observed.

Keywords: Heavy quarkonia, Belle experiment

1. Introduction

We report results obtained on Belle [1] experiment operates at the KEKB asymmetric-energy e^+e^- collider [2]. We use a 711 fb^{-1} data sample collected at the $\Upsilon(4S)$ resonance and a 118 fb^{-1} data sample collected at $\sqrt{s} = 10.867$ GeV. The Belle detector is described elsewhere [1].

2. Observation of a new charged charmonium-like state in $\bar{B}^0 \to J/\psi K^-\pi^+$ decays

We select events of the type $\bar{B}^0 \to J/\psi K^-\pi^+$ (where inclusion of charge-conjugate modes is always implied), with the J/ψ meson reconstructed via its e^+e^- and $\mu^+\mu^-$ decay channels. The selection procedure is described in Ref. [4]. The beam-energy-constrained mass of the B meson is defined as $M_{\rm bc} = \sqrt{E^2_{\rm beam} - (\sum_i \vec{p}_i)^2}$, where $E_{\rm beam}$ is the beam energy in the center-of-mass frame and $\vec{p}_i$ are the momenta of the decay products in the same frame. We require $|M_{\rm bc} - m_B| < 7$ MeV/c^2, where m_B is the B^0 mass. A mass-constrained fit is applied to the B meson candidates.

The Dalitz plot for the signal region is shown in Fig. 1(a). The most prominent features are the vertical bands due to the production of intermediate $K^*(892)$ and $K^*_2(1430)$ resonances. The Dalitz plot for the sidebands is shown in Fig. 1(b), where the events primarily accumulate in the lower left corner where the momentum of pions is low.

The amplitude of the decay $\bar{B}^0 \to J/\psi(\to \ell^+\ell^-)K^-\pi^+$ is represented as the sum of Breit-Wigner contributions for different intermediate two-body states. We perform an unbinned maximum likelihood fit over the four-dimensional space Φ. The masses and widths of all the K^* resonances except $K^*_0(800)$ are fixed to their nominal values. The mass and width of the $K^*_0(800)$ are fixed to the fit results in the default model without a Z_c^+ (M = 931 ± 21 MeV/c^2, Γ = 578 ± 49 MeV); the case of free mass and width is included in the systematic uncertainty. The mass M and the width Γ of the $Z_c(4430)^+$ are free parameters.

A search for a Z_c^+ with arbitrary mass and width is performed. The considered spin-parity hypotheses are $J^P = 0^-$, 1^-, 1^+, 2^- and 2^+. The 0^+ combination is forbidden by parity conservation in $Z_c^+ \to J/\psi\pi^+$ decays. The fit results for the Z_c^+ mass, width and significance in the default model are shown in Table 1. The global significance with the systematic uncertainty is 6.2σ. Thus,

Email address: krokovny@inp.nsk.su (Pavel Krokovny)

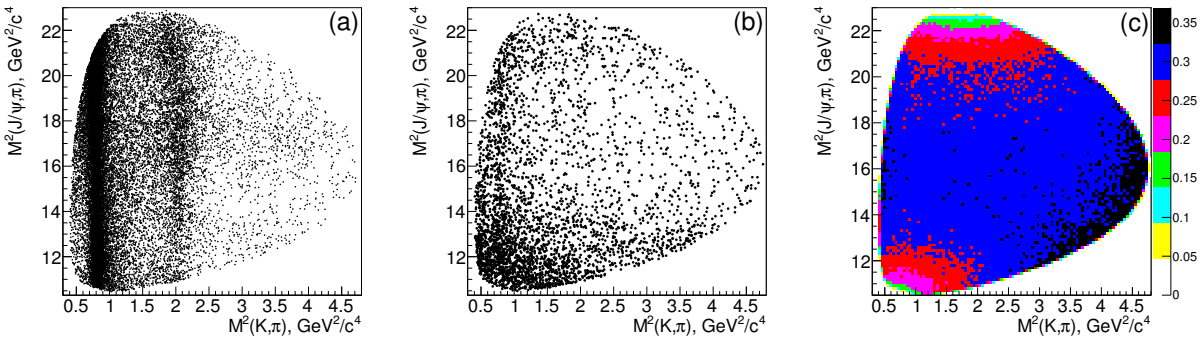

Figure 1: Dalitz plots of the signal region (a), sidebands (b) and signal efficiency (c).

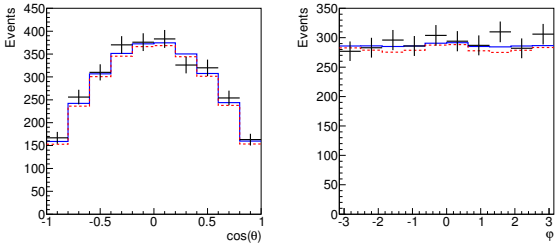

Figure 3: Projections of the fit results with (solid line) and without (dashed line) the $Z_c(4200)^+$ ($J^P = 1^+$) onto the angular variables in the default model for the region defined by $M^2_{K\pi} > 1.2\,\mathrm{GeV}^2/c^4$, $16\,\mathrm{GeV}^2/c^4 < M^2_{J/\psi\pi} < 19\,\mathrm{GeV}^2/c^4$. Points with error bars are data.

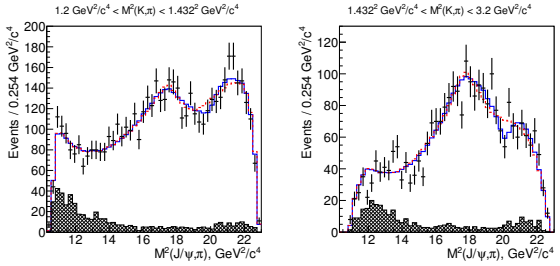

Figure 4: The fit results with (solid line) and without (dashed line) the $Z_c(4430)^+$ (the $Z_c(4200)^+$ is included in the model).

a new Z_c^+ state is observed. In the following, this state is referred to as the $Z_c(4200)^+$. The preferred spin-parity hypothesis is 1^+. The significance of the $Z_c(4430)^+$ with the systematic uncertainty is 4.0σ. Thus we find evidence for a new decay channel of the $Z_c(4430)^+$.

The amplitude absolute values and phases in the default model are listed in Table 2.

We also consider other amplitude models: without one of the insignificant K^* resonances [$K^*(1680)$, $K_0^*(1950)$]; with the addition of S-, P- and D-wave nonresonant $K^-\pi^+$ amplitudes; with free Blatt-Weisskopf r parameters; with free masses and widths of K^* resonances and with the LASS amplitudes instead of Breit-Wigner amplitudes for all spin-0 K^* resonances.

The significances of the $Z_c(4200)^+$ for all models other than the default are shown in Table 4. The minimal Wilks significance for the 1^+ hypotheses is 6.6σ; the corresponding global significance is 6.2σ.

The exclusion levels of the spin-parity hypotheses ($J^P = j^p$, $j^p \in \{0^+, 1^-, 2^-, 2^+\}$) for the default model are calculated using MC simulation. We generate MC pseudoexperiments in accordance with the fit result with the j^p $Z_c(4200)^+$ signal in data and fit them with the j^p and 1^+ signals. The resulting distribution of $\Delta(-2\ln L) = (-2\ln L)_{J^P=j^p} - (-2\ln L)_{J^P=1^+}$ is fitted to an asymmetrical Gaussian function and the p-value is calculated as the integral of the fitting function normalized to 1 from the value of $\Delta(-2\ln L)$ in data to $+\infty$. The results are presented in Table 5.

We also generate MC pseudoexperiments in accordance with the fit results for the 1^+ hypothesis, fit them with the j^p and 1^+ signals and obtain the distribution of $\Delta(-2\ln L)$. This distribution is fitted to an asymmetrical Gaussian function and the confidence level of the 1^+ hypothesis is calculated as the integral of the fitting function normalized to 1 from $-\infty$ to the value of $\Delta(-2\ln L)$ in data. The resulting confidence levels are shown in Table 5.

For models other than the default, we do not use the calculation of exclusion levels of the spin-parity hypotheses based on MC pseudoexperiments. Instead, the significance of the 1^+ hypothesis over the j^p hypothe-

Table 1: Fit results in the default model. Errors are statistical only.

J^P	0^-	1^-	1^+	2^-	2^+
Mass, MeV/c^2	4318 ± 48	4315 ± 40	4196^{+31}_{-29}	4209 ± 14	4203 ± 24
Width, MeV	720 ± 254	220 ± 80	370 ± 70	64 ± 18	121 ± 53
Significance (Wilks)	3.9σ	2.3σ	8.2σ	3.9σ	1.9σ

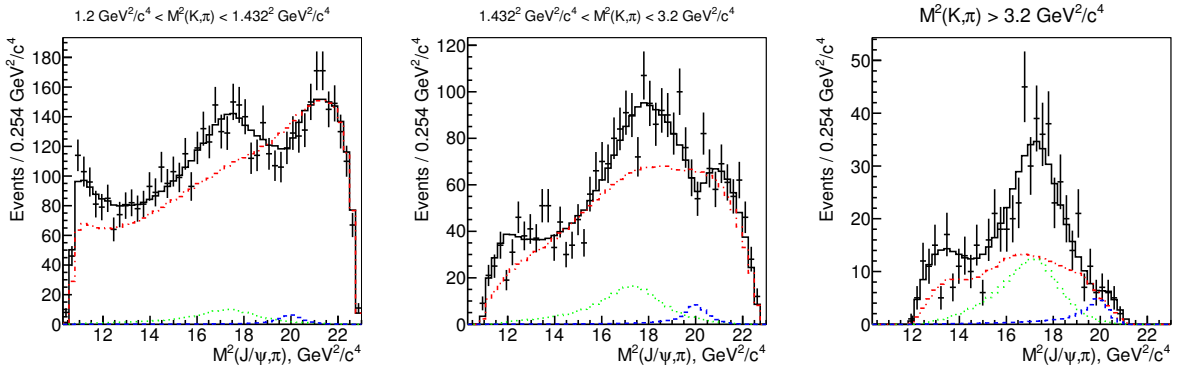

Figure 2: The fit results with the $Z_c(4200)^+$ ($J^P = 1^+$) in the default model. The points with error bars are data; the solid histograms are fit results, the dashed histograms are the $Z_c(4430)^+$ contributions, the dotted histograms are the $Z_c(4200)^+$ contributions and the dash-dotted histograms are contributions of all K^* resonances.

Table 2: The absolute values and phases of the helicity amplitudes in the default model for the 1^+ spin-parity of the $Z_c(4200)^+$. Errors are statistical only.

Resonance	$\lvert H_0\rvert$	arg H_0	$\lvert H_1\rvert$	arg H_1	$\lvert H_{-1}\rvert$	arg H_{-1}
$K_0^*(800)$	1.12 ± 0.04	2.30 ± 0.04	—	—	—	—
$K^*(892)$	1.0 (fixed)	0.0 (fixed)	0.844 ± 0.010)	3.14 ± 0.03	0.196 ± 0.014	-1.70 ± 0.07
$K^*(1410)$	0.119 ± 0.027	0.81 ± 0.26	0.123 ± 0.038	-1.04 ± 0.26	0.036 ± 0.039	0.67 ± 1.06
$K_0^*(1430)$	0.890 ± 0.028	-2.17 ± 0.05	—	—	—	—
$K_2^*(1430)$	4.66 ± 0.18	-0.32 ± 0.05	4.65 ± 0.18	-3.05 ± 0.08	1.26 ± 0.23	-1.92 ± 0.20
$K^*(1680)$	0.139 ± 0.043	-2.46 ± 0.31	0.082 ± 0.048	-2.85 ± 0.49	0.161 ± 0.056	1.88 ± 0.28
$K_3^*(1780)$	16.8 ± 3.6	-1.43 ± 0.24	19.1 ± 4.5	2.03 ± 0.31	10.2 ± 5.2	1.55 ± 0.62
$K_0^*(1950)$	0.241 ± 0.060	-2.39 ± 0.25	—	—	—	—
$K_2^*(1980)$	4.53 ± 0.74	-0.26 ± 0.16	3.78 ± 0.98	3.08 ± 0.28	3.51 ± 1.03	2.63 ± 0.34
$K_4^*(2045)$	590 ± 136	-2.66 ± 0.23	676 ± 164	0.06 ± 0.25	103 ± 174	-1.03 ± 1.62
$Z_c(4430)^+$	1.12 ± 0.32	-0.31 ± 0.26	1.17 ± 0.46	0.77 ± 0.25	$H_{-1} = H_1$	
$Z_c(4200)^+$	0.71 ± 0.37	2.14 ± 0.40	3.23 ± 0.79	3.00 ± 0.15	$H_{-1} = H_1$	

Table 3: The fit fractions and significances of all resonances in the default model ($J^P = 1^+$).

Resonance	Fit fraction	Significance (Wilks)
$K_0^*(800)$	$(7.1^{+0.7}_{-0.5})\%$	22.5σ
$K^*(892)$	$(69.0^{+0.6}_{-0.5})\%$	166.4σ
$K^*(1410)$	$(0.3^{+0.2}_{-0.1})\%$	4.1σ
$K_0^*(1430)$	$(5.9^{+0.6}_{-0.4})\%$	22.0σ
$K_2^*(1430)$	$(6.3^{+0.3}_{-0.4})\%$	23.5σ
$K^*(1680)$	$(0.3^{+0.2}_{-0.1})\%$	2.7σ
$K_3^*(1780)$	$(0.2^{+0.1}_{-0.1})\%$	3.8σ
$K_0^*(1950)$	$(0.1^{+0.1}_{-0.1})\%$	1.2σ
$K_2^*(1980)$	$(0.4^{+0.1}_{-0.1})\%$	5.3σ
$K_4^*(2045)$	$(0.2^{+0.1}_{-0.1})\%$	3.8σ
$Z_c(4430)^+$	$(0.5^{+0.4}_{-0.1})\%$	5.1σ
$Z_c(4200)^+$	$(1.9^{+0.7}_{-0.5})\%$	8.2σ

Table 4: Model dependence of the $Z_c(4200)^+$ Wilks significance.

Model	0^-	1^-	1^+	2^-	2^+
w/o $K^*(1680)$	3.2σ	3.1σ	8.4σ	3.7σ	1.9σ
w/o $K_0^*(1950)$	3.6σ	2.8σ	8.6σ	5.0σ	2.6σ
LASS	3.8σ	1.0σ	6.6σ	5.2σ	2.3σ
Free m and Γ	2.4σ	1.6σ	7.3σ	4.6σ	1.9σ
Free r	5.0σ	2.6σ	8.4σ	4.5σ	0.9σ
N.r. A(S)	3.8σ	2.9σ	7.9σ	4.1σ	2.0σ
N.r. A(S,P)	3.7σ	2.4σ	7.7σ	3.7σ	1.4σ
N.r. A(S,P,D)	4.1σ	2.3σ	7.7σ	3.8σ	1.3σ

sis is estimated as $\sqrt{\Delta(-2\ln L)}$. The comparison of the two methods for the default model is shown in Table 5. The formula-based calculation results in smaller values of the significance than the MC-based calculation, and thus it provides a conservative estimate of the significance. The results for all models are shown in Table 6. The 1^+ hypothesis is favored over the 0^-, 1^-, 2^-, 2^+ hypotheses at the levels of 6.1σ, 7.4σ, 4.4σ and 7.0σ, respectively.

We perform a search for the $Z_c(3900)^+$, using the amplitude model with the $Z_c(4200)^+$ ($J^P = 1^+$) as a null

Table 5: Exclusion levels of the $Z_c(4200)^+$ spin-parity hypotheses and confidence levels of the 1^+ hypothesis for the default model.

J^p	MC	$\sqrt{\Delta(-2\ln L)}$	1^+ C. L.
0^-	8.6σ	7.9σ	26%
1^-	9.8σ	8.7σ	48%
2^-	8.8σ	7.6σ	40%
2^+	10.6σ	8.8σ	42%

Table 6: Exclusion levels of the $Z_c(4200)^+$ spin-parity hypotheses.

Model	0^-	1^-	2^-	2^+
w/o $K^*(1680)$	8.5σ	8.5σ	8.0σ	9.0σ
w/o $K_0^*(1950)$	8.4σ	8.8σ	7.3σ	8.9σ
LASS	6.1σ	7.4σ	4.4σ	7.0σ
Free m and Γ	7.6σ	7.9σ	5.9σ	7.8σ
Free r	7.4σ	8.7σ	7.5σ	9.2σ
N.r. A(S)	7.6σ	8.1σ	7.2σ	8.5σ
N.r. A(S,P)	7.4σ	8.1σ	7.2σ	8.4σ
N.r. A(S,P,D)	7.2σ	8.1σ	7.1σ	8.4σ

hypothesis.All quantum number hypotheses with $J \leq 2$ are considered ($J^P \in \{0^+, 1^-, 1^+, 2^- 2^+\}$). We limit the mass and the width of the $Z_c(3900)^+$ in the same way as for the $Z_c(4430)^+$. No significant signal is found.

3. Observation of $e^+e^- \to \pi^+\pi^-\pi^0\chi_{bJ}$ and search for $X_b \to \omega\Upsilon(1S)$ at $\sqrt{s} = 10.867$ GeV

We study the $e^+e^- \to \pi^+\pi^-\pi^0\chi_{bJ}$ ($J = 0, 1, 2$) processes with subsequent $\chi_{bJ} \to \gamma\Upsilon(1S)$, $\Upsilon(1S) \to \ell^+\ell^-$ ($\ell = e$ or μ) decays. The selection criteria is described in [3]. The $\Upsilon(1S)$ candidate is reconstructed from a pair of oppositely-charged leptons. The χ_{bJ} candidates are reconstructed from a candidate $\Upsilon(1S)$ and a photon. The $\gamma\Upsilon(1S)$ invariant mass distribution after event selection is shown in Fig. 5, where the shaded histogram is from the normalized non-π^0 background events. Clear peaking signals in the χ_{b1} and χ_{b2} mass regions are observed.

An unbinned extended maximum likelihood fit is applied to the $\gamma\Upsilon(1S)$ mass spectrum with Crystal Ball functions as χ_{bJ} signal shapes and a first-order polynomial function as a background shape. Figure 5 shows the fit results. The statistical significance of the signal is estimated from the difference of the logarithmic likelihoods, $-2\ln(L_0/L_{\rm max})$, where L_0 and $L_{\rm max}$ are the likelihoods of the fits without and with a signal component, respectively. The signal significances of χ_{b1} and χ_{b2} are 12σ and 5.9σ with systematic uncertainties included, while the χ_{b0} signal is not significant. The fit results are summarized in Table 7. The Born cross section is calculated using $\sigma_B = N \cdot |1-\Pi|^2/[\mathcal{L}\cdot\mathcal{B}_{\rm int}\cdot\epsilon\cdot(1+\delta)]$, where N is the signal yield, $\mathcal{L}$ is the integrated luminosity, $\mathcal{B}_{\rm int}$ is the product of the branching fractions of the intermediate states to the reconstructed final states, ϵ is the corresponding detection efficiency, $1+\delta$ is the radiative correction factor and $|1-\Pi|^2$ is the vacuum polarization factor. In the MC simulation, trigger efficiency is included, and initial state radiation is taken into account

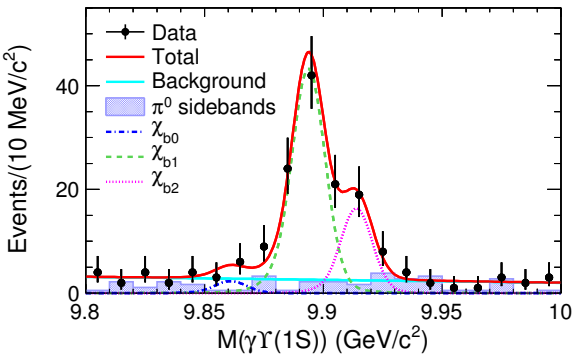

Figure 5: The $\gamma\Upsilon(1S)$ invariant mass distribution for selected $e^+e^- \to \pi^+\pi^-\pi^0\gamma\Upsilon(1S)$ candidate events. The shaded histogram is from normalized π^0-sideband events. The solid curves are the best fit for the total fit and background shape; the dash-dotted, dashed and dotted curves represent the χ_{b0}, χ_{b1} and χ_{b2} signals, respectively.

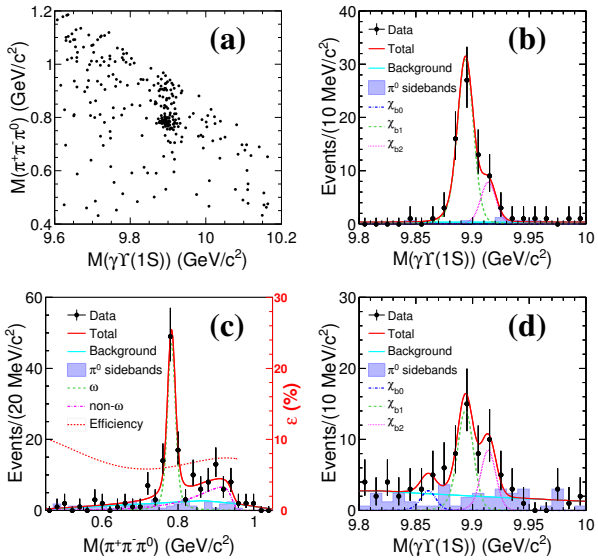

Figure 6: (a) The scatter plot of $M(\pi^+\pi^-\pi^0)$ versus $M(\gamma\Upsilon(1S))$ for selected $e^+e^- \to \pi^+\pi^-\pi^0\gamma\Upsilon(1S)$ candidate events; and (b) the projections to $M(\pi^+\pi^-\pi^0)$ for 9.8 GeV/c^2 <$M(\gamma\Upsilon(1S))$<10 GeV/c^2, where the dashed and dash-dotted curves represent the ω and $(\pi^+\pi^-\pi^0)_{\text{non}-\omega}$ events; the dotted curve shows the efficiency dependence on $M(\pi^+\pi^-\pi^0)$. Projections of $M(\gamma\Upsilon(1S))$ (c) in the ω signal region and (d) outside of ω signal region, where the dash-dotted, dashed and dotted curves represent the χ_{b0}, χ_{b1} and χ_{b2} signals, respectively. The solid curves are the best fit for the total signal and background shapes. The shaded histograms are from the normalized π^0 sideband events.

by assuming the cross sections follow the $\Upsilon(10860)$ line shape with a zero non-resonant contribution. The radiative correction factor $1+\delta$ is 0.65 ± 0.05; the value of $|1-\Pi(s)|^2$ is 0.929. The calculated branching fraction $\mathcal{B}$ for each mode is also shown in Table 7, where the total number of $\Upsilon(10860)$ events is $(4.02 \pm 0.20)\times10^7$ using $\sigma_{b\bar{b}} \equiv \sigma(e^+e^- \to b\bar{b}) = (0.340 \pm 0.016)$ nb and assuming all the $b\bar{b}$ events are from $\Upsilon(10860)$ resonance decays.

Figure 6(a) shows the scatter plot of $M(\pi^+\pi^-\pi^0)$ versus $M(\gamma\Upsilon(1S))$. Besides the clear ω signal in the χ_{bJ} mass region, there is an obvious accumulation of events above the ω mass region. Hereinafter, we denote these events as $(\pi^+\pi^-\pi^0)_{\text{non}-\omega}$ events.

An unbinned two-dimensional (2D) extended maximum likelihood fit to the $\pi^+\pi^-\pi^0$ versus $\gamma\Upsilon(1S)$ mass distributions is applied to extract the $\omega\chi_{bJ}$ and $(\pi^+\pi^-\pi^0)_{\text{non}-\omega\chi_{bJ}}$ yields. In this fit, Crystal Ball functions are used for the χ_{bJ} signal shapes, a Breit-Wigner function and an Argus function (both are convoluted with a Gaussian resolution function) represent the ω and $(\pi^+\pi^-\pi^0)_{\text{non}-\omega}$ shapes, respectively, and a linear function is used for the backgrounds. The Gaussian resolution function is obtained from MC simulation.

Figures 6(b-d) show the $\pi^+\pi^-\pi^0$ mass projection for 9.8 GeV/c^2 < $M(\gamma\Upsilon(1S))$ < 10 GeV/c^2, and the $\gamma\Upsilon(1S)$ mass projection within and outside the ω signal region (0.753 GeV/c^2 < $M(\pi^+\pi^-\pi^0)$ < 0.813 GeV/c^2), where the shaded histograms are from the normalized π^0 sideband events. Clear χ_{b1} and χ_{b2} signals can be seen in the $\gamma\Upsilon(1S)$ invariant mass spectrum, while no excess of χ_{b0} events above expected backgrounds is observed.

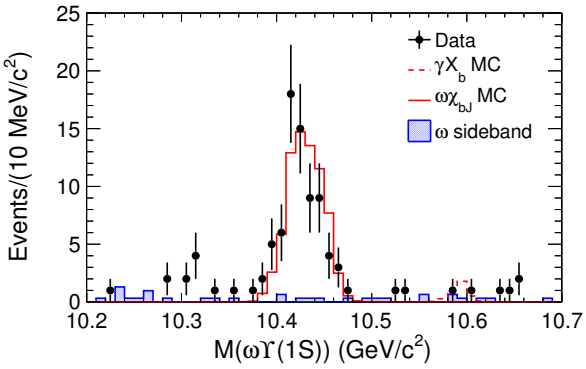

Figure 7: The $\omega\Upsilon(1S)$ invariant mass distribution. The dots with error bars are from data, the solid histogram is from the normalized contribution of $e^+e^- \to \omega\chi_{bJ}$ (J = 0, 1, 2) from MC simulation and the shaded histogram is from normalized ω mass sideband events. The dashed histogram is from the MC signal sample $e^+e^- \to \gamma X_b \to \gamma\omega\Upsilon(1S) \to \gamma\pi^+\pi^-\pi^0\ell^+\ell^-$ at $\sqrt{s}$ = 10.867 GeV with X_b mass fixed at 10.6 GeV/c^2 and yield fixed at the upper limit at 90% C.L.

Table 7: Fitted signal yield, signal significance (Σ), detection efficiency (ε), Born cross section (σ_B), branching fraction ($\mathcal{B}$) and relative systematic uncertainty ($\sigma^{(1)}_{\rm sys}$ for Born cross section and $\sigma^{(2)}_{\rm sys}$ for branching fraction).

Mode	Yield	Σ (σ)	ε (%)	σ_B (pb)	$\mathcal{B}$ (10^{-3})	$\sigma^{(1)}_{\rm sys}$ (%)	$\sigma^{(2)}_{\rm sys}$ (%)
$\pi^+\pi^-\pi^0\chi_{b0}$	< 13.6	1.0	6.43	< 3.1	< 6.3	25	24
$\pi^+\pi^-\pi^0\chi_{b1}$	80.1 ± 9.9	12	6.61	$0.90 \pm 0.11 \pm 0.13$	$1.85 \pm 0.23 \pm 0.23$	14	12
$\pi^+\pi^-\pi^0\chi_{b2}$	28.6 ± 6.5	5.9	6.65	$0.57 \pm 0.13 \pm 0.08$	$1.17 \pm 0.27 \pm 0.14$	14	12
$\omega\chi_{b0}$	< 7.5	0.5	6.35	< 1.9	< 3.9	29	28
$\omega\chi_{b1}$	59.9 ± 8.3	12	6.53	$0.76 \pm 0.11 \pm 0.11$	$1.57 \pm 0.22 \pm 0.21$	14	13
$\omega\chi_{b2}$	12.9 ± 4.8	3.5	6.56	$0.29 \pm 0.11 \pm 0.08$	$0.60 \pm 0.23 \pm 0.15$	26	25
$(\pi^+\pi^-\pi^0)_{\rm non-}\omega\chi_{b0}$	< 10.7	0.4	6.68	< 2.3	< 4.8	41	41
$(\pi^+\pi^-\pi^0)_{\rm non-}\omega\chi_{b1}$	23.6 ± 6.4	4.9	6.88	$0.25 \pm 0.07 \pm 0.06$	$0.52 \pm 0.15 \pm 0.11$	21	20
$(\pi^+\pi^-\pi^0)_{\rm non-}\omega\chi_{b2}$	15.6 ± 5.4	3.1	6.91	$0.30 \pm 0.11 \pm 0.14$	$0.61 \pm 0.22 \pm 0.28$	45	45

The fit results with the calculated Born cross sections and branching fractions are summarized in Table 7.

We search for the $X(3872)$-like state X_b in the process $e^+e^- \to \gamma X_b$ with $X_b \to \omega\Upsilon(1S)$ at $\sqrt{s} = 10.867$ GeV. The selection criteria are the same as in $e^+e^- \to \pi^+\pi^-\pi^0\chi_{bJ}$. Figure 7 shows the $\omega\Upsilon(1S)$ invariant mass distribution with the requirement of $M(\pi^+\pi^-\pi^0)$ within the ω signal region; we search for the X_b from 10.55 to 10.65 GeV/c^2. No X_b signal is observed after applying all the event selection criteria. With the detection efficiency of 8.1% and assuming that the observed signals come from $\Upsilon(10860)$ decays, we obtain the product branching fraction $\mathcal{B}(\Upsilon(10860) \to \gamma X_b)\mathcal{B}(X_b \to \omega\Upsilon(1S)) < 2.9 \times 10^{-5}$ at 90% C.L.

4. Summary

An amplitude analysis of $\bar{B}^0 \to J/\psi K^-\pi^+$ decays in four dimensions has been performed. A new charged charmonium-like state $Z_c(4200)^+$ decaying to J/ψ and π^+ is observed with the significance of 6.2σ. The minimal quark content of this state is exotic: $|c\bar{c}u\bar{d}\rangle$. Its mass and width are measured to be $M = 4196^{+31+17}_{-29-13}$ MeV/c^2 and $\Gamma = 370^{+70+70}_{-70-132}$ MeV. The preferred quantum number assignment is $J^P = 1^+$. Other hypotheses with $J^P \in \{0^-, 1^-, 2^-, 2^+\}$ are excluded at the levels of 6.1σ, 7.4σ, 4.4σ and 7.0σ, respectively. Also, evidence for a new decay channel $\to J/\psi\pi^+$ of the $Z_c(4430)^+$ is found.

We observe clear $\pi^+\pi^-\pi^0\chi_{b1}$ and $\pi^+\pi^-\pi^0\chi_{b2}$ signals, while no significant $\pi^+\pi^-\pi^0\chi_{b0}$ signal is found. In the $\pi^+\pi^-\pi^0$ invariant mass spectrum, besides a clear ω signal, significant non-ω signals are also observed. We also search for the $X(3872)$-like state, X_b with a hidden $b\bar{b}$ component decaying into $\omega\Upsilon(1S)$, in $\Upsilon(10860)$ radiative decay. No significant signal is observed for such a state with mass between 10.55 and 10.65 GeV/c^2.

We thank the KEKB group for excellent operation of the accelerator; the KEK cryogenics group for efficient solenoid operations; and the KEK computer group, the NII, and PNNL/EMSL for valuable computing and SINET4 network support. We acknowledge support from MEXT, JSPS and Nagoya's TLPRC (Japan); ARC and DIISR (Australia); FWF (Austria); NSFC, the Fundamental Research Funds for the Central Universities YWF-14-WLXY-013 and CAS center for Excellence in Particle Physics (China); MSMT (Czechia); CZF, DFG, and VS (Germany); DST (India); INFN (Italy); MOE, MSIP, NRF, GSDC of KISTI, BK21Plus, and WCU (Korea); MNiSW and NCN (Poland); MES, RFAAE and RFBR grant 14-02-01220 (Russia); ARRS (Slovenia); IKERBASQUE and UPV/EHU (Spain); SNSF (Switzerland); NSC and MOE (Taiwan); and DOE and NSF (USA). We acknowledge support from MinES of RF (grant 14.610.21.0002, identification number RFMEFI61014X0002).

References

[1] A. Abashian *et al.* (Belle Collaboration), Nucl. Instrum. Methods Phys. Res. Sect. A **479**, 117 (2002); also see detector section in J. Brodzicka *et al.*, Prog. Theor. Exp. Phys. **2012**, 04D001 (2012).

[2] S. Kurokawa and E. Kikutani, Nucl. Instrum. Methods Phys. Res. Sect. A **499**, 1 (2003), and other papers included in this Volume; T. Abe *et al.*, Prog. Theor. Exp. Phys. **2013**, 03A001 (2013) and following articles up to 03A011.

[3] X. H. He *et al.*, Phys.Rev.Lett. **113**, 142001 (2014).

[4] K. Chilikin *et al.*, arhiv:1408.6457[hep-ex], submitted to Phys.Rev. D.